Materials Science & Engineering A 960 (2026) 150130

Contents lists available at ScienceDirect

Materials Science & Engineering A

journal homepage: www.elsevier.com/locate/msea

# On the critical temperature required for grain boundary sliding in Nickel bicrystal: A micromechanical approach

Divya Sri Bandla [a], Subin Lee [a,b,*], Christoph Kirchlechner [a]

[a] Institute for Applied Materials, Karlsruhe Institute of Technology, Karlsruhe, 76131, Germany
[b] Karlsruhe Nano Micro Facility (KNMFi), Karlsruhe Institute of Technology, Hermann-von-Helmholtz-Platz 1, 76344, Eggenstein-Leopoldshafen, Germany

A B S T R A C T

Despite several decades of research on grain boundary sliding and its fundamental mechanisms, two questions remain: What is the critical temperature at which a grain boundary begins to slide, and what is its physical significance? Here, we determine the critical temperature for grain boundary sliding in a high-angle Ni grain boundary by employing an *in situ* high temperature micropillar compression in a scanning electron microscope (SEM). Regardless of the high melting point of Ni, grain boundary sliding was observed to initiate in the range of 250–300 °C (0.30–0.33 $T_m$) for 1 μm-diameter micropillars. The size-dependent mechanical response of micropillars indicates that the observed grain boundary sliding is a dislocation-mediated process. A comparison with nanocrystalline Ni from the literature suggests that the observed sliding temperature can be considered as the critical temperature required for unconstrained sliding. We propose that this critical temperature corresponds to the onset of lattice dislocation dissociation into grain boundary dislocations.

## 1. Introduction

Grain boundary sliding (GBS) is a phenomenon in which grains slide relative to each other along the grain boundary under externally applied stresses. High homologous temperatures (>0.5 $T_m$, $T_m$ is the absolute melting temperature), slow strain rates ($10^{-5}$ to $10^{-2}$ $s^{-1}$), and fine grain sizes (≤10 μm) are preferable for GBS in polycrystalline materials [1–5]. These conditions are necessary for triggering diffusion and dislocation-dominating processes in the vicinity of grain boundary compared to the grain interior. A significant advantage of GBS is superplasticity or high strain rate sensitivity (>0.3), which has been observed to impart good mechanical formability to both metallic materials and ceramics [6,7]. However, GBS can also be a damaging process by inducing cavities during the service of a material, resulting in premature failure [8,9].

In literature, GBS of polycrystals has been categorized into two types, Lifshitz and Rachinger sliding. In the former case, GBS occurs as an accommodation mechanism for diffusion creep (either Nabarro-Herring or Coble creep) to avoid void formation between grains [10,11]. In Rachinger sliding, GBS itself is an independent mechanism that occurs with the aid of dislocation activity [12]. To quantify the significance of GBS compared to plastic deformation within the grains, a marker line approach has been developed [13,14]. In which a line is marked across the grain boundary, and sliding (both Lifshitz and Rachinger) causes an offset in the marker line during deformation, thus enabling the quantification of strain caused by GBS. Studies showed that the contribution of GBS to total deformation can be as high as 80% [15,16].

Apart from a quantitative understanding, polycrystalline materials pose a difficulty in the qualitative fundamental mechanism of GBS. This is due to the triple junction points in polycrystals at which an additional accommodation mechanism is required for GBS to progress [17–19]. This accommodation mechanism can act as a limiting step, also limiting the current understanding of the (unconstrained) grain boundary sliding process. Moreover, the presence of various grain boundaries (such as random high-angle grain boundaries, coincidence site lattice boundaries, and twin boundaries) in polycrystals complicates the understanding of the influence of grain boundary character on GBS. Therefore, to gain a more fundamental understanding of the GBS processes, bicrystals have been used as a model system with well-defined grain boundary geometries.

Studies on bicrystals revealed mechanistic details of GBS, based on which diffusion and dislocation-based mechanisms for GBS were proposed. Here, it is necessary to know that these proposed mechanisms in bicrystals act independently and do not require any additional slip mechanism for accommodation, unlike the processes in polycrystals. Thus, bicrystals help to understand the fundamentals of GBS. Diffusion-based mechanism, also known as 'pure GBS', involves transport of matter from one part of the boundary to another via diffusion [20,21]. The sliding rate depends on grain boundary diffusion and defects (ledges or steps) along the grain boundary [22]. Dislocation-based GBS, which is

* Corresponding author. Institute for Applied Materials, Karlsruhe Institute of Technology, Karlsruhe, 76131, Germany.
*E-mail address:* subin.lee@kit.edu (S. Lee).

https://doi.org/10.1016/j.msea.2026.150130
Received 21 December 2025; Received in revised form 24 February 2026; Accepted 19 March 2026
Available online 20 March 2026

also referred to as 'stimulated GBS', involves the glide and climb of grain boundary dislocations along the grain boundary [23,24]. These grain boundary dislocations (GBDs) are believed to result from the dissociation of lattice dislocations (LDs), and are therefore linked to the occurrence of in-grain slip activity [24,25]. This dissociation was found to be sensitive to the grain boundary character, where high-energy grain boundaries were more favorable for dissociation compared to low-energy special boundaries, such as the coincidence site lattice boundaries [26,27]. Thus, imparting high resistance to GBS in the latter case.

These diffusion and dislocation-based mechanisms were also confirmed by experimental observations on bicrystals of Zn [28] and Cd [29]. In crystals unfavorable for in-grain dislocation slip, GBS was observed to occur through diffusion without in-grain slip activity, whereas in the case of grain orientations favoring in-grain slip, GBS followed the dislocation-based mechanism. Nevertheless, the extent of sliding and the sliding rate are higher for the dislocation-mediated mechanism than the diffusion mechanism [29]. A theoretical model proposed on the dislocation-mediated GBS mechanism highlighted that the sliding rate depends on the GBD density [30]. However, it should be noted that in the case of dislocation-mediated GBS, in-grain slip can also be detrimental. An experimental study on Cu bicrystals observed that, depending on the orientation of in-grain slip and its interaction with the grain boundary, there was a formation of ledges at the grain boundary, which led to nucleation of cavities and fracture [8]. Furthermore, a compatible in-grain slip between two grains of bicrystal, which is favorable for slip transmission, was observed to suppress GBS [31].

Regardless of thorough knowledge of the mechanisms and factors influencing GBS, a question remains: Is there a critical temperature required to activate GBS of a particular grain boundary? This question is not only fundamental in understanding GBS mechanisms, but it is also important to understand the susceptibility of a grain boundary to undergo sliding and to tailor microstructures to switch on/off GBS selectively. In this study, therefore, we employed *in situ* micro-scale mechanical testing, a technique well-suited for understanding the deformation behavior of various microstructural features, such as grain boundaries [32,33] and precipitates [34,35]. Test protocols using focused ion beam milling (FIB) to prepare micropillars in bulk crystals and small-scale loading rigs based on nanoindentation transducers to perform compression tests are well developed [36–38]. The adaptation of micro-scale testing revealed new insights into the GBS mechanism. In a study on β-Sn bicrystals, micropillars prepared at the grain boundary showed dislocation-mediated GBS at room temperature [39]. However, the GBS was found to be influenced by mechanical size effects, where the resistance to GBS increased with an increase in pillar diameter. In another study on Al, also noted GBS at room temperature [40]. However, the proposed mechanism for GBS is neither diffusion nor dislocation based. It is purely from an energy balance argument, where the energy required to create a new surface from sliding is balanced by the recovered elastic energy.

Despite probing into GBS at the micro scale, these studies do not answer the critical temperature required for the sliding of a particular grain boundary. Therefore, in the current study, the deformation behavior of Ni bicrystal micropillars with a high-angle grain boundary (HAGB) was systematically studied varying testing temperatures to determine the critical temperature required for GBS. Also, the influence of mechanical size effects on the sliding behavior and the extent of sliding compared to the in-grain slip is quantified by employing the conventional marker line approach at the micron scale. The findings of the current study revealed the fundamental mechanistic differences in the sliding behavior of polycrystalline and bicrystalline materials, suggesting a critical temperature required for the dislocation dissociation into grain boundary and imparting sliding along the grain boundary.

## 2. Materials and methods

### 2.1. Preparation of Ni bicrystal micropillars

A Ni bicrystal with a HAGB was prepared using the Bridgman method. A small piece with a size of 7 × 3 mm was sliced from the prepared bicrystal using a diamond saw and mechanically ground to 4000-grit sandpaper, followed by polishing with diamond suspension (9, 3, and 1 μm). Finally, the sample was subjected to vibropolishing (Vibromet, Buehler, Germany) with non-crystallizing colloidal silica suspension of particle size 0.02 μm for 2 h.

The crystallographic orientation of the two grains in the bicrystalline sample was determined using an electron backscattered detector (EBSD, Symmetry S2, Oxford Instrument) equipped to a FIB-SEM system (Crossbeam 550L, Zeiss). The sample was tilted at 70° angle and scanned by an electron beam with an acceleration voltage of 30 kV, probe current of 5 nA, and working distance of 13 mm for EBSD analysis. Micropillars of diameters ($d$) 1, 3, and 6 μm were prepared along the grain boundary using a $Ga^+$ ion FIB (Crossbeam 550L, Zeiss). An acceleration voltage of 30 kV was used for FIB milling. An annular milling technique was used to fabricate micropillars with circular cross-section. The milling was performed in a three-step sequence in an outside-to-inside direction. The detailed parameters are listed in Table 1.

The milling pattern was placed in the vicinity of the grain boundary to capture the grain boundary in the middle of the pillar. The height-to-diameter aspect ratio of pillars was maintained between 2 and 2.5. A vertical line (marker line) was marked on pillars with FIB for quantitative characterization of GBS, i.e., determination of activation stress for GBS and the contribution of GBS to the total applied strain. An acceleration voltage of 30 kV with 50 pA current was used for 6 μm pillars, whereas 10 pA current was used for 3 μm and 1 μm pillars to mark the vertical line.

### 2.2. In situ SEM high temperature micropillar compression

*In situ* micropillar compression tests were carried out by Bruker Hysitron PI89 indenter in an SEM (Merlin, Zeiss) in displacement-controlled mode over a temperature range from room temperature (RT) to 300 °C at a strain rate of $10^{-3}$ $s^{-1}$. Flat punches (diamond for RT and tungsten carbide for high temperature tests) of diameters 2, 5, and 10 μm from Synton MDP were used to test 1, 3, and 6 μm pillars, respectively. The PI89 indenter was equipped with a high-load transducer capable of a maximum load of 0.5 N, a noise floor of 10 μN, and a maximum displacement of 150 μm.

Both the tip and sample heaters were heated independently at a rate of 10 °C/min and were stabilized at the target temperature for 30 min. Before proceeding with the micropillar compression tests, contact was made between the flat punch and the sample surface to ensure both were at the same test temperature with temperature stability of ±0.1 °C, and to minimize heat flow between the flat punch and the sample. 7 to 10

**Table 1**
FIB milling parameters used to fabricate micropillars of different diameters.

| Pillar diameter (μm) | Step | Parameters | | | |
|---|---|---|---|---|---|
| | | Ion currents (nA) | Repeats | Dose (nC μm$^{-2}$) | Dwell time (μs) |
| 1 | Coarse | 7.0 | 152 | 4.00 | 100 |
| | Intermediate | 1.5 | 89 | 3.50 | 100 |
| | Fine | 0.1 | 2 | 1.06 | 130 |
| 3 | Coarse | 30.0 | 63 | 15.00 | 100 |
| | Intermediate | 1.5 | 4 | 5.00 | 130 |
| | Fine | 0.7 | 2 | 2.70 | 410 |
| 6 | Coarse | 30.0 | 105 | 24.00 | 150 |
| | Intermediate | 7.0 | 30 | 7.50 | 150 |
| | Fine | 1.5 | 5 | 4.90 | 200 |

micropillars were tested for each test condition. In the micropillar stress-strain curves, the yield stress was considered as the stress required to create a 2% plastic strain.

### 2.3. Microstructure characterization of deformed micropillars

The deformed micropillars were observed under a transmission electron microscope (TEM, Themis 300, Thermo Fisher Scientific) operating at 300 kV. For the TEM analysis, the lamella containing a micropillar was prepared through FIB milling (Crossbeam 550L). Firstly, the micropillar was covered with platinum and lifted out. It was then subjected to coarse milling at 30 kV and 300 pA to reduce the thickness to 1 μm and subsequently fine milling with 30 kV and 100 pA until 500 nm, 30 kV and 50 pA until 200 nm, and 30 kV and 20 pA until 100 nm. Finally, the lamella was cleaned with 5 kV-10 pA and 2 kV-10 pA.

## 3. Results

### 3.1. Characterization of Ni bicrystal

The crystallographic orientation of the Ni bicrystal was measured by EBSD, where the normal direction of one grain is along the [344] direction and the other one is along the [324] direction (see Fig. 1a). The misorientation of the two grains at the random HAGB is approximately 20°. The grain boundary trace from FIB cross-sectional view revealed that the boundary is passing through the sample at an angle of approximately 35° (Fig. 1b). A typical micropillar ($d = 1$ μm) prepared at the grain boundary is shown in Fig. 1c, with the grain boundary indicated by yellow arrows. The compression axis is parallel to the sample normal direction (indicated by the black arrow in Fig. 1c), which means that the grain above the grain boundary was deformed under [324] direction, and the loading direction for the lower grain is close to [344] direction.

### 3.2. Determination of favorable conditions for the sliding of a HAGB

To determine the required temperature for sliding of a HAGB in Ni, micropillar compression tests were performed on bicrystalline 1 μm sized pillars at $10^{-3}$ $s^{-1}$ strain rate over a range of temperatures from RT to 300 °C. The temperature was limited to 300 °C because grain boundary migration was observed in 1 μm pillars at 420 °C. Note that larger micro-pillars did not show this behavior at the same temperature.

Firstly, the bicrystalline micropillar deformed at RT showed no sign of GBS but two different slip traces in each grain (Fig. 2a). A slip trace analysis revealed the activation of $(1\bar{1}1)[011]$ and $(\bar{1}11)[101]$, in the [324] oriented grain with the Schmid factor ($m$) being 0.39 and 0.36, respectively, and $(1\bar{1}1)[011]$ and $(\bar{1}11)[110]$ with $m$ being 0.31 and 0.25 activated in the [344] oriented grain. The schematic of all the observed slip traces in the micropillar is shown in Fig. 2j. The pillars tested at 100 °C and 200 °C also showed a similar behavior as compared to pillars deformed at RT, with no sign of sliding but slip traces in both grains (Fig. 2b and c).

A sign of slip transmission (marked with a white dashed line in Fig. 2c) can be seen in the pillars deformed at RT (Fig. 2a), 100 °C (Fig. 2b), and 200 °C (Fig. 2c). The slip systems participated in slip transmission were identified to be $(1\bar{1}1)[011]$ in [324] grain and $(\bar{1}11)[110]$ in [344] grain. The slip transmission or compatibility of slip between adjacent grains is indicated with a factor called the slip transmission factor ($m'$), which can be expressed as $\cos\phi \cos k$, where $\phi$ is the angle between the normal to slip planes, and $k$ is the angle between slip directions [41]. The slip systems that are parallel in adjacent grains show a high degree of slip transmission with high $m'$, whereas the orthogonal slip systems are incompatible for slip transmission and result in a low $m'$ value. In support of the evidence of slip transmission in the deformed pillars from RT to 200 °C, the slip plane $(1\bar{1}1)$ in [324] and $(\bar{1}11)$ in [344] are nearly parallel with an inclination angle of 16° and $m'$ of 0.95. The other slip systems are almost orthogonal and result in low $m'$, as listed in Fig. 2k.

With an increment in temperature from 200 °C to 250 °C, in addition to the slip activity in both grains, a sign of GBS was noted (marked by a white dashed ellipse in Fig. 2d). A further increase in temperature to 275 °C resulted in mixed observations of GBS: the sliding was less pronounced in one pillar (Fig. 2e), similar to the pillar deformed at 250 °C, while the other pillar exhibited increased sliding, as shown in Fig. 2f.

At 300 °C, all the tested pillars exhibited prominent GBS, where the [324] grain was sheared with respect to [344] grain along the grain boundary (Fig. 2g). Along with the GBS behavior, the micropillar also showed slip traces in both top and bottom grains that are similar to the pillars deformed at lower temperatures, however, no signs of slip transmission can be found with the resolution provided by post-mortem SEM imaging. It should be noted that freshly milled micropillars were used for testing at each temperature, with different pillars tested at each temperature. The above results indicate that the critical temperature to activate the sliding of a HAGB in a Ni bicrystal micropillar of 1 μm diameter is in the range of 250 °C (first signs of GBS visible) to 300 °C (all pillars show significant GBS). Since the occurrence of GBS appears to be in a transition regime up to 275 °C, the further tests were conducted at 300 °C, where GBS was unambiguously observed. At this temperature, the effect of pillar diameter on GBS was investigated by testing micropillars with a diameter of 3 and 6 μm at $10^{-3}$ $s^{-1}$ strain rate. The corresponding secondary electron images of deformed pillars with larger diameters are shown in Fig. 2h and i. GBS is evident in pillars of 3 and 6 μm diameter, along with the slip traces similar to those of 1 μm pillar

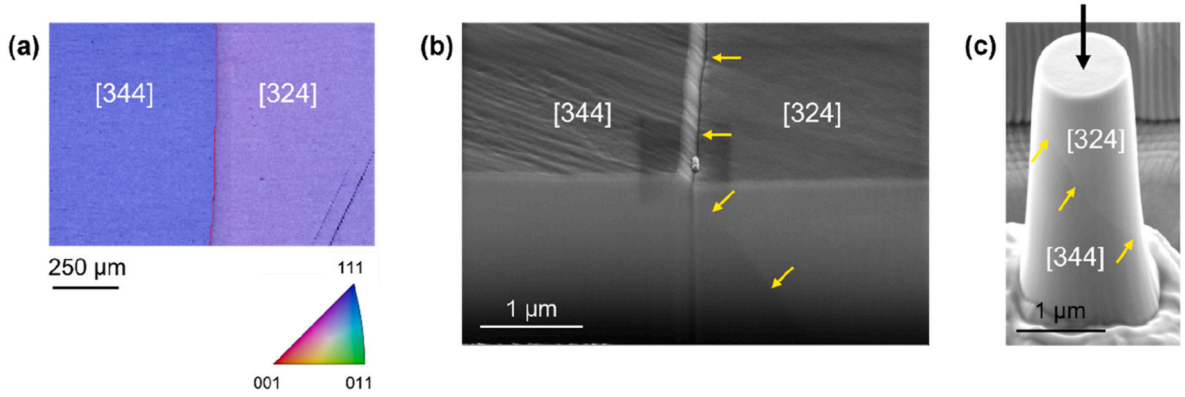


**Fig. 1.** (a) EBSD inverse pole figure (in Z-direction) map of the Ni bicrystal. (b) Cross-section view of Ni bicrystal showing the trace of grain boundary with yellow arrows, and (c) a typical bicrystal micropillar with the grain boundary. The black arrow represents the loading direction of the pillar. (For interpretation of the references to color in this figure legend, the reader is referred to the Web version of this article.)

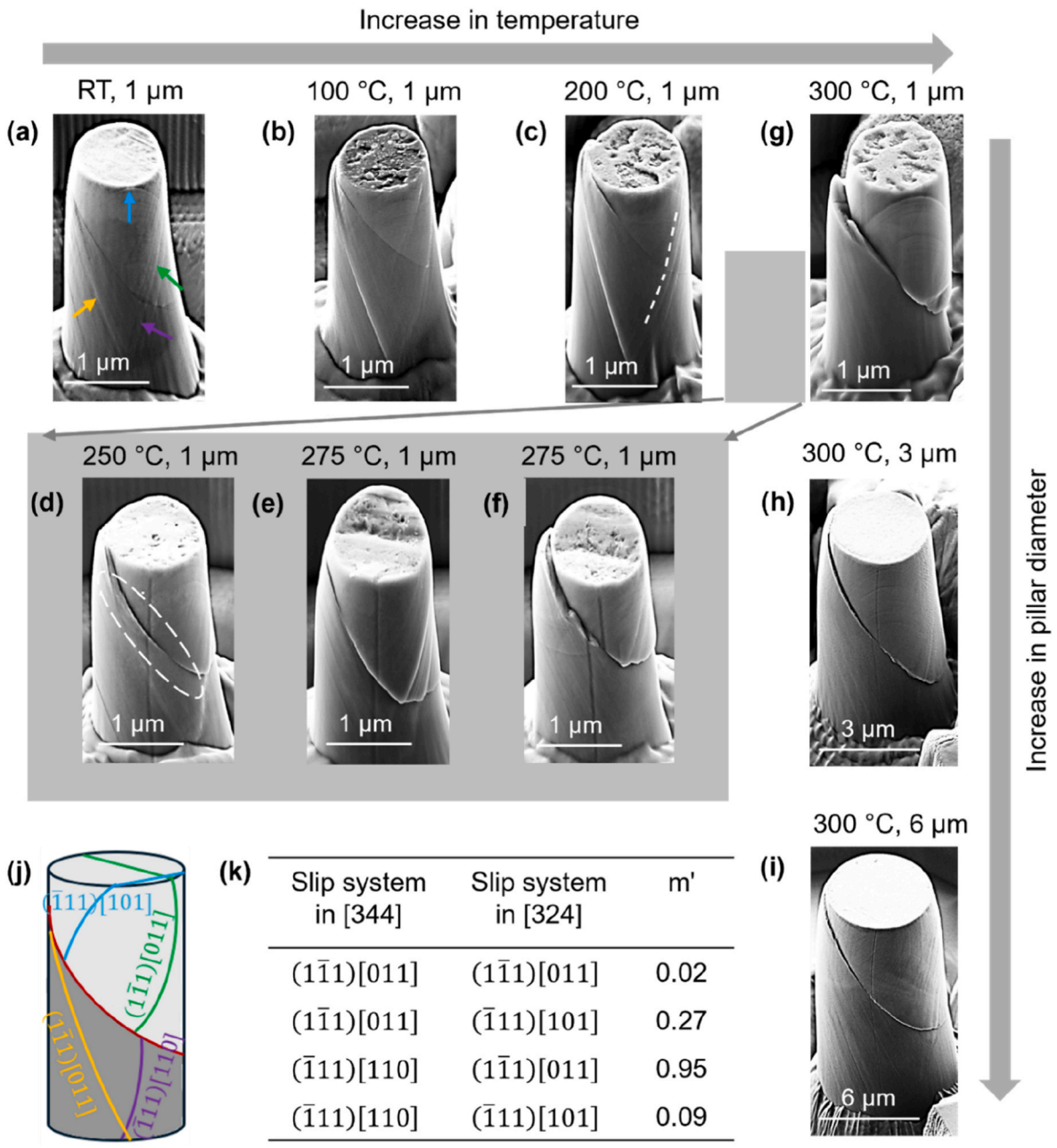


| Slip system in [344] | Slip system in [324] | m' |
|---|---|---|
| $(1\bar{1}1)[011]$ | $(1\bar{1}1)[011]$ | 0.02 |
| $(1\bar{1}1)[011]$ | $(\bar{1}11)[101]$ | 0.27 |
| $(\bar{1}11)[110]$ | $(1\bar{1}1)[011]$ | 0.95 |
| $(\bar{1}11)[110]$ | $(\bar{1}11)[101]$ | 0.09 |

**Fig. 2.** Secondary electron images of micropillars of 1 μm diameter deformed to the strain of 0.1 with $10^{-3}$ $s^{-1}$ strain rate at (a) RT, (b) 100 °C, (c) 200 °C, (d) 250 °C, (e) and (f) 275 °C, and (g) 300 °C. (h) and (i) are the images of 3 and 6 μm pillars, respectively deformed at 300 °C and $10^{-3}$ $s^{-1}$. (j) is the schematic of activated slip systems in Ni bicrystal micropillar during compression. The grain boundary represented by red color and the color codes of slip traces follow the color code in (a). (k) is listing the slip transmission factor values between the slip systems activated in both grains. (For interpretation of the references to color in this figure legend, the reader is referred to the Web version of this article.)

(Fig. 2g).

The stress-strain curves of two pillars with 1 μm diameter tested at RT and 300 °C are presented in Fig. 3a. The 2% offset yield strength of Ni bicrystal micropillars reduced from 700 MPa at RT to 450 MPa at 300 °C with the activation of GBS. It should also be noted that there is an intentional unloading segment at 5% strain to minimize lateral stresses caused during laterally constrained micropillar compression.

Fig. 3b represents the stress-strain curves of bicrystal micro pillars of diameter 1, 3, and 6 μm tested at 300 °C and $10^{-3}$ $s^{-1}$, highlighting mechanical size effects (i.e. the smaller is stronger paradigm) in the presence of GBS. These size effects are particularly dominant when the sample dimensions fall within the range of microstructural length scales, which is typically below 10 μm for metallic micropillars [42]. The size effect is quantified by the size exponent ($n$), which can be determined from the slope of yield strength against pillar diameter on a log-log scale, as shown in Fig. 4. Along with the yield strength data of bicrystal micropillars, the data of single crystal micropillars from [344] and [324] grains are also gathered in this plot. At RT, the size exponent was determined to be −0.65 and −0.72 for [344] and [324] grains, respectively.

Blue half-filled squares in Fig. 4 indicate the yield strength of bicrystalline micropillars at RT. It lies between the strengths of the two single grain micropillars. Since the upper part of the bicrystal pillar, where stress is localized and the initial plastic deformation starts, is oriented along [324], its yield strength is expected to be similar to that of [324] single crystals, but is slightly higher. This increase may arise

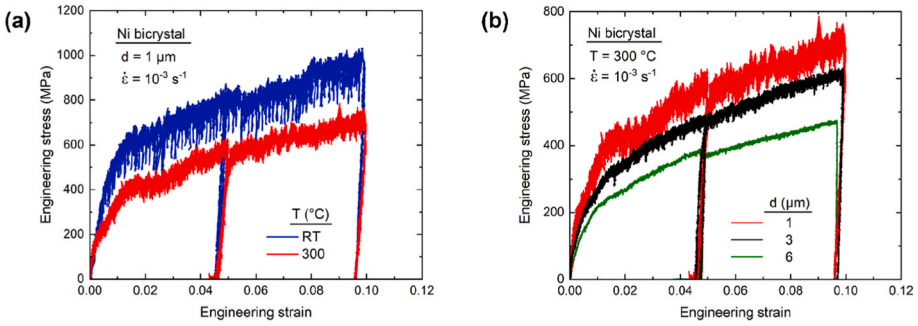


**Fig. 3.** Representative stress-strain curves of Ni bicrystal (a) 1 μm pillars deformed with strain rate of $10^{-3}$ $s^{-1}$ at RT and 300 °C and (b) pillars of diameter 1, 3, and 6 μm deformed at $10^{-3}$ $s^{-1}$ and 300 °C.

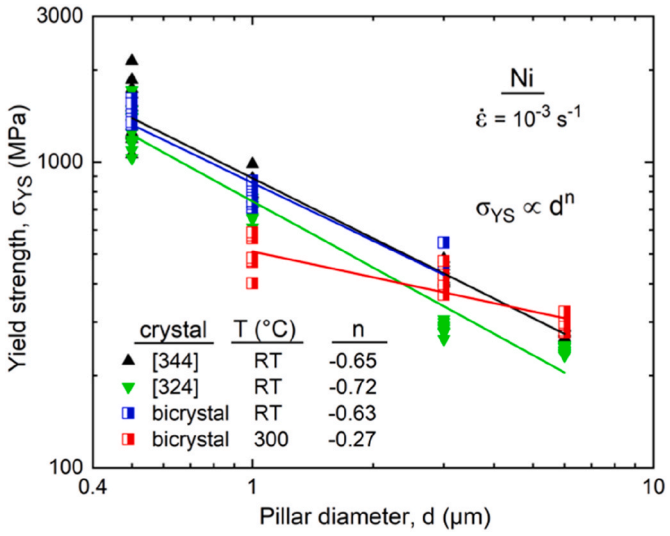


**Fig. 4.** Log-log plot of yield strength as a function of pillar diameter of Ni [344] and [324] grains at RT and Ni bicrystal at RT and 300 °C to determine the size exponent.

from the presence of the grain boundary limiting the dislocation source size [43].

The size exponent of the bicrystalline pillars at RT was measured to be −0.63, which is comparable to those of the [344] and [324] grains. The red half-filled squares in Fig. 4 represent the bicrystal data obtained at 300 °C. At this temperature, the size exponent is reduced to −0.27, showing a clear deviation from the value observed at RT. This discrepancy suggests that a different deformation mechanism becomes active at elevated temperature. Based on slip trace analysis from the *in situ* videos, it can be concluded that GBS contributes to reducing the external size dependence of yield strength at high temperatures, although a notable size effect persists.

### 3.3. Quantitative characterization of GBS

An attempt has been made to employ the conventional marker line approach on micropillars to determine the strain from GBS ($\varepsilon_{GBS}$) and the critical stress ($\tau_{GBS}$) required to activate the sliding behavior. Fig. 5a presents the bicrystalline micropillar of 3 μm diameter, where the grain boundary is indicated with yellow arrows and the vertical marker line produced by the FIB is specified with green arrows. In the micropillar subjected to deformation at RT, the marker line is undisturbed at the intersection of grain boundary and marker line (Fig. 5b and c). It indicates that the deformation is primarily accommodated by dislocation plasticity in the grains. Some slip traces are observed to extend across the grain boundary, indicating the occurrence of slip transfer (white dashed line in Fig. 5c). Nevertheless, the marker line remains largely unaffected even in such cases.

Whereas the micropillar deformed at 300 °C showed a clear offset in the marker line, as indicated by the yellow bar in Fig. 5e. A distinct step along the grain boundary also formed, suggesting the activation of GBS. Despite the occurrence of GBS, fine slip traces are still observed in both the upper and lower grains.

Upon successful observation of offset in marker line for 3 μm diameter pillars due to GBS, this approach was also applied to 1 μm and 6 μm pillars. Fig. 6a–c presents the secondary electron images of pillars from 1 μm to 6 μm diameter, and the offset in the marker line is highlighted by the yellow bar. The offset corresponds to a displacement of the top grain in the x-direction, as shown by $\Delta x$ in the schematic Fig. 6d. From the measurable quantities $\Delta x$ and $\theta$, the displacement produced in the y-direction or loading direction, due to GBS, can be calculated as $\Delta y = \Delta x \tan\theta$. The strain produced by GBS is thus determined as, $\varepsilon_{GBS} = \Delta y / L$, where $L$ is the height of the micropillar before deformation.

$\varepsilon_{GBS}$ divided by the total applied strain in the micropillar compression test ($\varepsilon_{total}$) gives the contribution of GBS to the total applied strain, $\varepsilon_{GBS}/\varepsilon_{total}$. It has been determined for pillars of 1, 3, and 6 μm and plotted in Fig. 6e. Despite showing GBS activation at similar temperature over a wide range of pillar diameters, the contribution of GBS differs with pillar diameter. Multiple micropillar compression tests for each pillar diameter showed that, on average, GBS contributes ~49 ± 4% of the total applied strain for 1 μm pillars. It decreased to ~25 ± 4% and ~18 ± 1% for 3 μm and 6 μm pillars, respectively. This observation is similar to the mechanical size effect presented in Fig. 4, where an increase in pillar diameter resulted in a decrease in yield strength. Thus, it can be suggested that the reduction in GBS contribution to the total applied strain may be related to the intrinsic mechanical size effect associated with micropillars, causing higher stresses for smaller pillars.

The grain boundary region upon sliding is no longer smooth, but several irregularities are noticed in all the micropillars as indicated by white arrows in Fig. 6a–c. These irregularities may be due to the intersection of slip planes with the grain boundary during micropillar compression. As noted in the deformed micropillars from Fig. 2a–i, each grain has several slip traces that belong to two independent activated slip systems (Fig. 2j). Thus, during deformation, the grain boundary is intersected by slip traces belonging to four different slip systems, which may result in the formation of irregularities.

The marker line method is also used to determine the $\tau_{GBS}$ by correlating the changes observed in the marker line during the deformation to the stress-strain response. Fig. 7 represents the engineering stress-strain curve of a 3 μm bicrystalline pillar deformed at 300 °C (black curve) and the corresponding micrographs of the pillar at different applied strain levels. The marker line remains undisturbed in the elastic deformation region. However, shortly after entering the plastic deformation region, at an applied strain of 1.2%, a slight offset in the marker line becomes noticeable, as indicated by the white dashed circle in micrograph 2. This suggests the activation of GBS and the

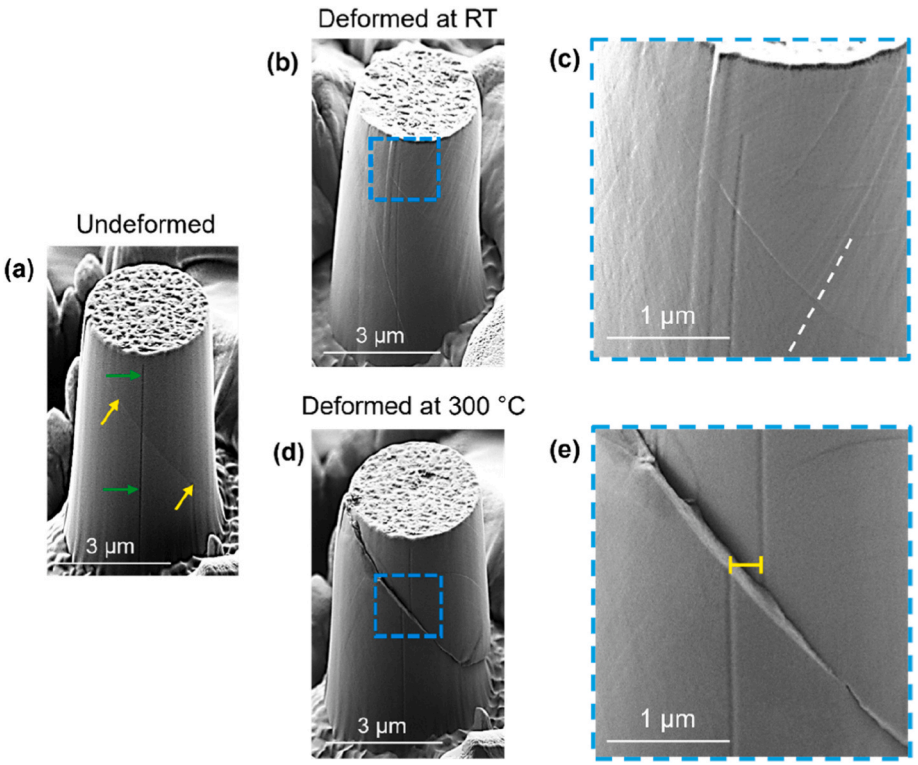


**Fig. 5.** (a) is the undeformed Ni bicrystal micropillar with the grain boundary indicated by yellow arrows and vertical marker line indicated by green arrows. (b) is after deformation at RT and (c) is high magnification image of (b) highlighting no change in vertical marker line and slip transfer activity with white dashed line. (d) is the micropillar deformed at 300 °C and (e) is the corresponding high magnification image showing an offset in the marker line by yellow bar. (For interpretation of the references to color in this figure legend, the reader is referred to the Web version of this article.)

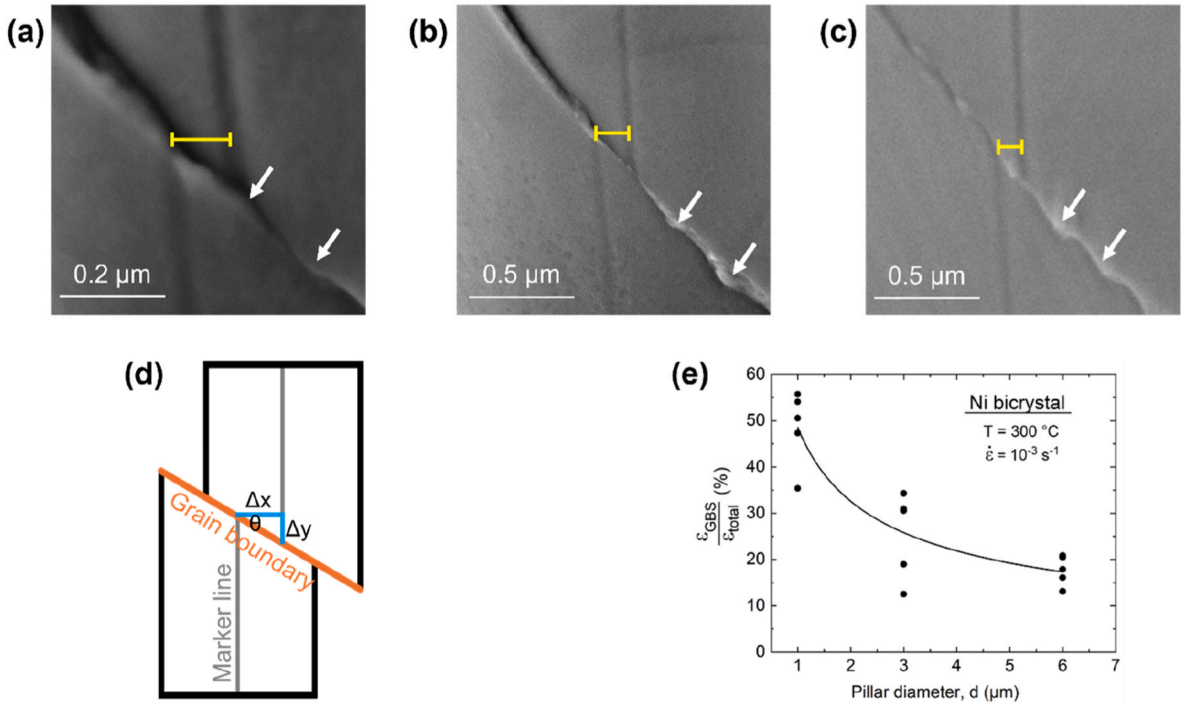


**Fig. 6.** Micropillars of diameter (a) 1 μm, (b) 3 μm, and (c) 6 μm showing an offset in marker line due to GBS deformation at 300 °C and $10^{-3}$ $s^{-1}$. Offset in marker line is highlighted by yellow bar and the irregularities along the grain boundary are marked by white arrows. (d) is the schematic demonstrating the calculation of GBS contribution to the total applied strain. (e) shows the variation in the contribution of GBS to the total applied strain with pillar diameter. (For interpretation of the references to color in this figure legend, the reader is referred to the Web version of this article.)

corresponding stress can be considered as the upper bound for the activation stress (engineering stress) required for GBS. This engineering

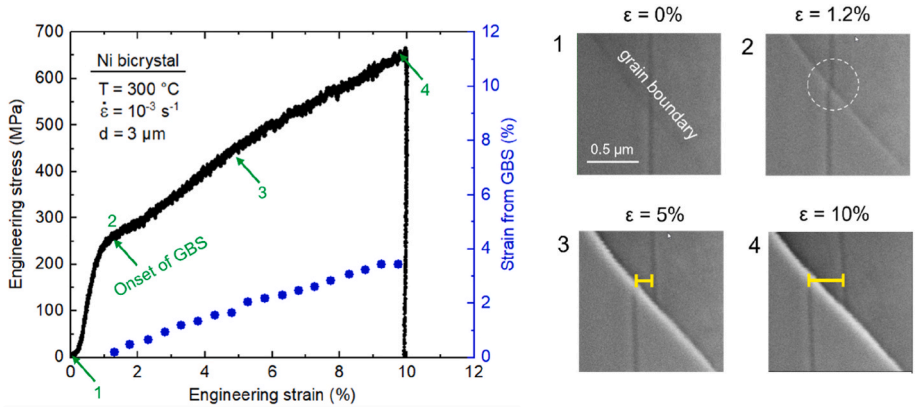


**Fig. 7.** The stress-strain curve of a 3 µm pillar underwent GBS at 300 °C and $10^{-3}$ $s^{-1}$. The data in blue-filled circles is the determined strain from GBS at different intervals of applied strain during the micropillar compression test. The SEM micrographs on the right side show the grain boundary and vertical marker line at different applied strain levels during the test, as indicated by the green arrows in the stress-strain curve. Micrograph 1 is at the start of test (ε = 0%), 2 is at the onset of GBS (ε = 1.2%), and 3 and 4 are at strain levels of 5% and 10%, respectively. (For interpretation of the references to color in this figure legend, the reader is referred to the Web version of this article.)

stress is multiplied by the cosine of angle between the loading axis and the grain boundary to determine the upper bound $\tau_{GBS}$. In this way, the activation stress required for sliding is determined for pillars and plotted in Fig. 8 (black diamond symbols) as a function of pillar diameter on log-log scale. The smallest pillar exhibits the highest upper bound for the activation stress for GBS, with a linear relation between $d$ and $\tau_{GBS}$, suggesting a power law relation similar to the size effect described in Fig. 4.

The *in situ* micropillar compression technique is also used to calculate the sliding rate of the grain boundary. For this, the offset in the marker line is measured at different strain intervals during the test (micrographs 3 and 4 in Fig. 7), and $\varepsilon_{GBS}$ is determined as described in Fig. 6d. The blue data points in Fig. 7 are the variation of $\varepsilon_{GBS}$ with the total applied strain. It can be seen that there is a constant linear increase in $\varepsilon_{GBS}$ throughout the deformation without any sign of slide hardening, i.e., no reduction in sliding rate.

### 3.4. Microstructure characterization after GBS

The microstructural changes of a 3 µm pillar deformed at 300 °C to a strain of 10% were characterized by TEM, as shown in Fig. 9. Both grains showed dislocation plasticity. Due to differences in diffraction conditions, the dislocation structure in the [344] grain appears less distinct than in the [324] grain in Fig. 9a. However, imaging under an alternative two-beam condition confirmed that the lower grain also contains a comparable number of dislocations. Apart from the dislocation structure, a local grain boundary curvature also can be seen, as marked with yellow arrows in Fig. 9a. Although it is not possible to determine whether this curvature was induced by deformation or pre-existed, it is expected that such local irregularities increase friction during grain boundary sliding.

A high-magnification image at the grain boundary (Fig. 9b) showed dislocations located at or intersecting the boundary, with some appearing to lie directly on the grain boundary plane. Notably, there is no evidence of dislocation pile-up or increased dislocation density in the vicinity of the boundary.

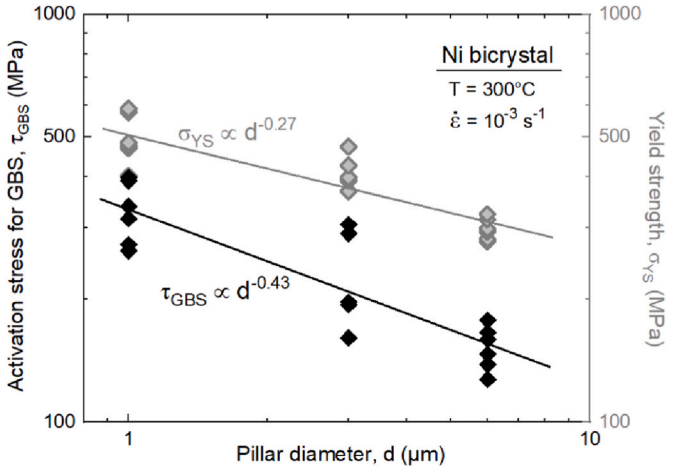


**Fig. 8.** Variation in the activation stress for GBS and yield strength with pillar diameter on a log-log scale for determining the size exponent. Each data point is from an individual micropillar compression experiment.

## 4. Discussion

### 4.1. Insights into the mechanistic details of GBS

GBS models proposed in the literature can broadly be categorized as either diffusion-based or dislocation-mediated models. Based on our observation, we suggest a dislocation-assisted sliding mechanism for a HAGB in Ni micropillar at the temperatures and strain rate tested here. In diffusion-based models, Ashby et al. [22] suggested that GBS can occur via the transport of matter along grain boundaries or through the bulk by volume diffusion, without dislocation slip. In contrast, all micropillars in the present study exhibited GBS activity only after attaining plastic strain, as presented in Fig. 7, indicating that slip activity is a prerequisite for GBS under the current experimental conditions. As noted in Fig. 8, despite enhanced surface diffusion in smaller pillars, which could potentially promote GBS at lower stresses, our results show the opposite trend: smaller pillars require higher activation stresses for sliding. This is inconsistent with classical diffusion-controlled mechanisms, where grain size and stress are linearly proportional [44,45]. The noted inverse relationship between pillar diameter and GBS activation stress suggests that the observed sliding behavior is not governed by a diffusion-based mechanism.

According to McLeans's model of dislocation-mediated GBS [24], the primary step is the production of LDs through slip activity within a grain interior. These LDs subsequently dissociate into GBDs upon reaching the grain boundary, as illustrated in Fig. 10. Since the Burgers vector of LD does not lie in the grain boundary plane, it dissociates into GBDs with Burgers vector parallel ($b_p$) and perpendicular ($b_n$) to the grain boundary. The GBD with $b_p$, glides along the grain boundary under the acting shear stress component, thus resulting in sliding phenomenon. In

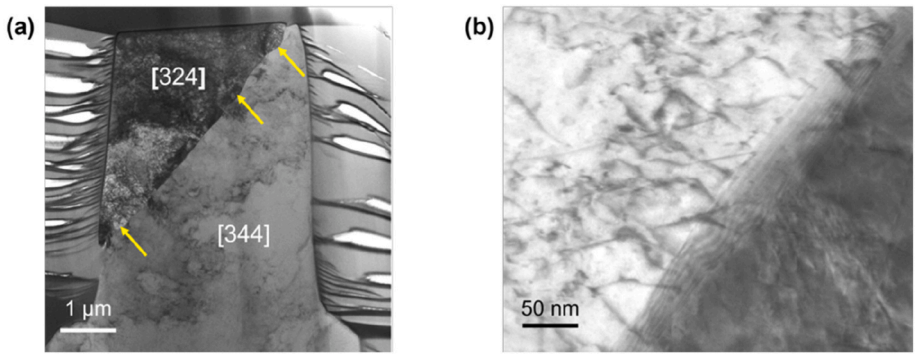


**Fig. 9.** (a) TEM bright field image of a 3 μm pillar that underwent sliding at 300 °C and $10^{-3}$ $s^{-1}$ and (b) is at high magnification showing the dislocations at grain boundary.

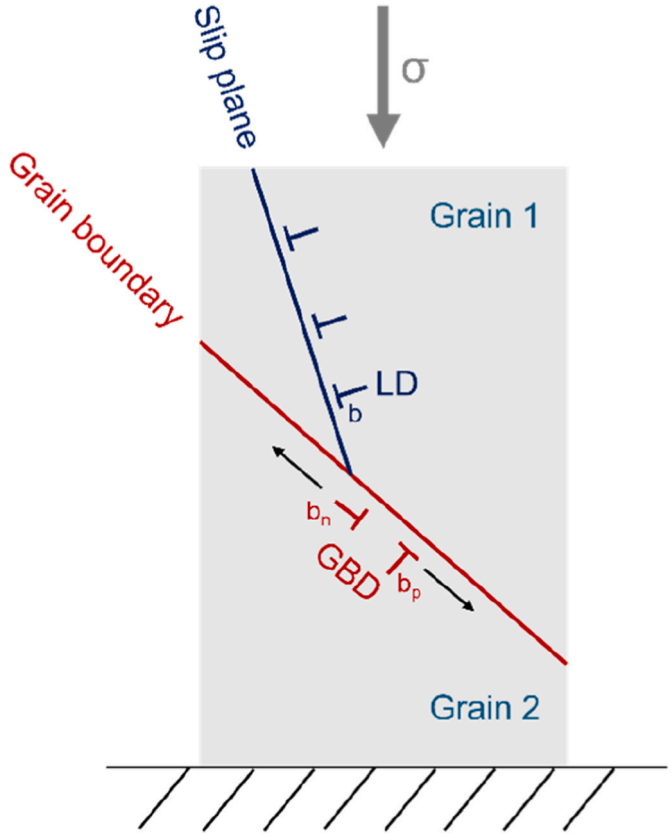


**Fig. 10.** A schematic illustration of dislocation-mediated GBS, highlighting the dissociation of LDs from slip into GBD at the grain boundary and further glide and climb motion of GBDs along the grain boundary.

support of this model, slip activity in the micropillars (Fig. 2) and dislocation activity at the grain boundary (Fig. 9b) can be seen clearly. Furthermore, the absence of a clear dislocation pile-up at the grain boundary in Fig. 9b implies continuous dislocation glide along the boundary, rather than accumulation, further corroborating the dislocation-mediated nature of GBS.

Another experimental observation supporting dislocation-mediated GBS is the size dependence in the GBS activation stress (Fig. 8). This size dependence is similar to mechanical size effects, where pillars with a smaller diameter showed the higher yield strength (Fig. 4). The mechanical size effects in micropillars are caused by the reduction in dislocation source size and source numbers with pillar diameter. Thus, the pillars with small diameter require large stress for slip or dislocation activity [42]. It can be suggested that the observed higher GBS activation stress for smaller pillar diameters may be due to the requirement of indeed slip activity in the micropillars.

Similarly, a size dependence is also noted in the contribution of GBS to the total strain (Fig. 6e). As discussed above, in the dislocation-mediated GBS process, sliding results from the glide of a dislocation along the grain boundary under acting shear stress components. Consequently, the extent of sliding is governed by the magnitude of shear stress acting on the boundary plane. Due to intrinsic mechanical size effects (Fig. 4), smaller pillars experience higher stresses than larger ones, resulting in a more pronounced contribution of GBS to the overall plastic strain in smaller diameter micropillars. Moreover, in dislocation-mediated GBS, $\varepsilon_{GBS}$ also depends on the availability of dislocation for gliding along the grain boundary. Owing to the stochastic variation of the number of dislocations from pillar to pillar in small micropillars, the micropillars with a small diameter are prone to show larger variation in $\varepsilon_{GBS}/\varepsilon_{total}$ compared to the large micropillars, as noticed in Fig. 6e.

It should be noted that in our experimental conditions, GBS was dominated by dislocation rather than diffusion-based mechanisms. This may be due to the low testing temperature (300 °C) employed in the current study, which suppressed the transport of matter from one part of the boundary to another via diffusion along the Ni grain boundary. However, a transition from dislocation to diffusion-based GBS mechanism may be expected at high temperature.

### 4.2. Unusual strain hardening during GBS

A study by Gong and Wilkinson on Sn [39] and Aitken et al. [40] on Al bicrystal micropillars showed strain softening during GBS. However, in contrast to those observations, the current study showed a pronounced strain hardening during GBS (Fig. 3b). One possibility for this discrepancy may be due to lateral compliance forces during micropillar compression testing. To confirm it, we conducted a micropillar compression at 300 °C by employing an unloading step at every 2% strain level, and the corresponding stress-strain curve is shown in Fig. 11. The strain hardening is apparent, suggesting the observed strain hardening phenomenon during GBS is not from the lateral force caused by the lateral stiffness of the system during the test. It is essential to consider that in Aitken et al. [40] work on Al bicrystals, the micropillars are prepared through $Ga^+$ ion FIB, which may cause segregation of $Ga^+$ ions to the grain boundary and embrittlement in Al [46]. This embrittlement could be the reason for the observed strain softening during GBS of Al.

Strain hardening is occasionally noted during superplastic flow in polycrystalline materials, especially with nano-sized grains at low temperatures [47,48]. Ovid'ko and Sheinerman [49] proposed a mechanism for strain hardening in nanocrystalline materials during dislocation-mediated GBS. According to them, during the GBS, the climb motion of grain boundary dislocations ($b_n$ from the dissociation of lattice dislocations in Fig. 10) along the boundary can change the tilt

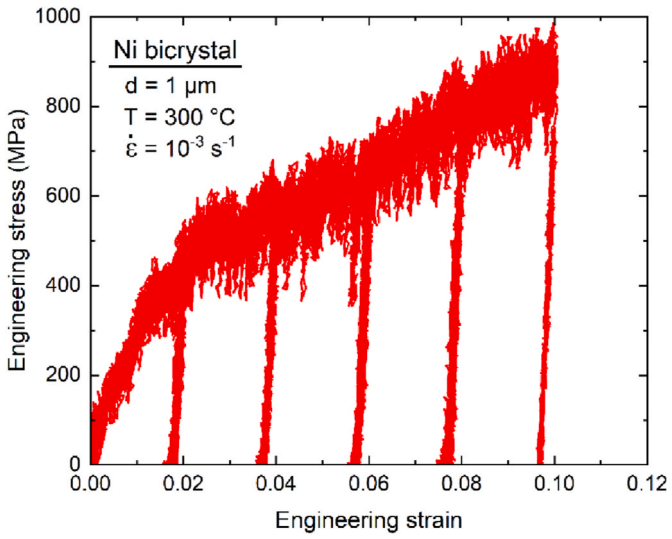


**Fig. 11.** Stress-strain curve of a 1 μm pillar subjected to multiple unloading conditions during deformation at 300 °C and $10^{-3}$ $s^{-1}$.

misorientation and create internal stresses, which cause strain hardening, especially at low temperatures. Partly, the dislocation-mediated GBS argument in the current study aligns with this proposed strain hardening mechanism. However, further grain boundary analysis after GBS is needed to confirm the reason behind the strain hardening.

Strain hardening during GBS may also result from local grain boundary curvature (Fig. 9b), which increases the stress required for sliding.

### 4.3. Critical temperature required for sliding along the grain boundary

In the current study, all bicrystalline Ni pillars showed sliding at 300 °C at a strain rate of $10^{-3}$ $s^{-1}$ over a pillar diameter range from 1 μm to 6 μm. The GBS temperature observed in this study is lower than that reported for nanocrystalline Ni (nc-Ni) by McFadden et al. [47]. This comparison is illustrated in Fig. 12, which shows the relationship between temperature and pillar diameter (or grain size), summarizing the GBS conditions from both studies. It can be noted that the GBS temperature observed in bicrystalline Ni is substantially lower than the one reported for nc-Ni. Moreover, a clear difference in grain size or pillar

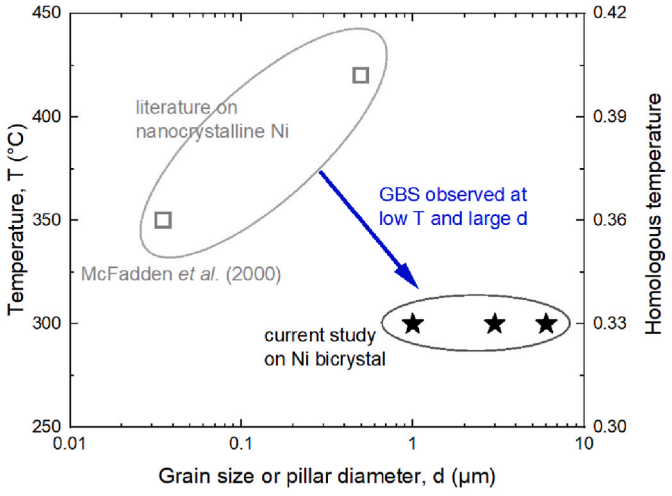


**Fig. 12.** Comparison between the GBS conditions observed in Ni bicrystal from the current study (filled star symbols) and the nanocrystalline Ni from the literature [50] (open square symbols) at a strain rate of $10^{-3}$ $s^{-1}$.

diameter can also be observed, where in Ni bicrystals, GBS is noticed in large pillar diameters (1, 3, and 6 μm) as compared to nano grains (40 and 500 nm) in nc-Ni.

An immediate reason one can claim for GBS at lower temperature and larger pillar diameter in bicrystal compared to nanocrystal is the relatively simple geometry in the former case, which is the absence of triple junction points [17]. The absence of triple junctions in bicrystalline pillars results in unconstrained slip, i.e. no backstress on GBS is caused by compatibility requirements; hence, no additional accommodating mechanisms (e.g. dislocation climb) are required for GBS in bicrystalline samples. Consequently, GBS in bicrystals involves only three steps: slip in the crystal to produce LDs, dissociation of LDs into GBDs at the grain boundary, and finally the glide of GBDs along that grain boundary under acting shear stress components [24]. From Fig. 2, the slip activity in the crystals can be seen at all tested temperatures, suggesting that slip in the crystal is independent of temperature. As observed by Ishida in Fe-Mn alloy [51] and supported by Watanabe group's work on Zn [26] and Al [27] bicrystals, the dissociation of LDs to GBDs at the grain boundary is a temperature-dependent process. Owing to the sign of GBS at temperatures from 250 to 300 °C (Fig. 2d–i), it can be said that at those temperatures, the LDs from slip activity are dissociated into GBDs. Finally, the glide of these GBDs along the grain boundary, which is aided by applied stress during micropillar compression, results in sliding. Thus, the observed sliding temperature in the current study (ranging from 250 °C to 300 °C) can be regarded as the critical temperature required for dislocation dissociation and subsequent sliding of dislocations along the HAGB in Ni, requiring no additional accommodating mechanism.

However, it should be noted that the observed parameters of unconstrained GBS (critical temperature, activation stress, and strain produced by GBS) in the current study may be sensitive to the material parameters like the character of the grain boundary and inclination angle between the grain boundary and the loading direction. A grain boundary with a different character (misorientation or grain boundary energy) demands a different critical temperature for sliding due to the difference in energy requirement for the dissociation of LDs to GBDs [25]. Whereas a grain boundary with similar character but a difference in inclination angle shows GBS at a similar critical temperature, with a variation in $\tau_{GBS}$ and $\varepsilon_{GBS}$. This may be due to the change in shear stress acting on the grain boundary plane, which influences the glide of GBDs along the grain boundary. Nevertheless, Ni bicrystal with only a change in the orientation of grains but not the inclination angle and character of grain boundary is expected not to show a pronounced difference in GBS parameters.

## 5. Conclusion

GBS can be activated in bicrystalline Ni micropillars at relatively low temperature and moderate strain rate. Unlike bulk polycrystalline materials, bicrystalline pillars do not require nano level diameters to activate low temperature sliding. In the current study, GBS is noticed at 300 °C in pillars of diameters ranging from 1 μm to 6 μm. This temperature, 300 °C, can be regarded as an upper bound for the critical temperature required for sliding in the absence of accommodation mechanism. This temperature may be needed for the dissociation of LDs into GBDs at the HAGB in Ni. Like mechanical size effects in micropillars, the activation stress for GBS is also found to be inversely related to pillar diameter. This observation along with the slip trace evidence in micropillar suggests that the GBS process is mediated through glide of dislocations along the grain boundary. The GBS process showed pronounced strain hardening with no sign of slide hardening.

## CRediT authorship contribution statement

**Divya Sri Bandla:** Writing – original draft, Visualization, Methodology, Investigation, Formal analysis, Data curation. **Subin Lee:** Writing

– review & editing, Supervision. **Christoph Kirchlechner:** Writing – review & editing, Supervision, Project administration, Funding acquisition, Conceptualization.

## Declaration of competing interest

The authors have declared no conflict of interest.

## Acknowledgement

The authors express their gratitude to the Deutsche Forschungsgemeinschaft (DFG) for its financial support within project 500076185 “Micromechanical characterization of grain boundary slip: Towards a deformation mechanism map”. We also acknowledge the support of the Karlsruhe Nano Micro Facility (KNMFi, www.knmf.kit.edu), a Helmholtz Research Infrastructure at Karlsruhe Institute of Technology (KIT, www.kit.edu).

## Data availability

Data will be made available on request.

## References

[1] M.J.N.V. Prasad, A.H. Chokshi, Superplasticity in electrodeposited nanocrystalline nickel, Acta Mater. 58 (2010) 5724–5736, https://doi.org/10.1016/j.actamat.2010.06.047.
[2] P.A. Martelli, I. Sabirov, M.A. Monclus, E. Bassini, G. Marchese, D. Ugues, The effect of temperature and strain rate on the grain boundary sliding in a CM247 LC Ni-based superalloy processed with laser based powder bed fusion, J. Mater. Res. Technol. 28 (2024) 2466–2477, https://doi.org/10.1016/j.jmrt.2023.12.131.
[3] J.-J. He, R. Sandström, S.-R. Lü, P. Korzhavyi, J. Zhang, H.-Y. Qin, J.-B. Liu, Predicting grain boundary sliding in metallic materials, Acta Mater. 286 (2025) 120718, https://doi.org/10.1016/j.actamat.2025.120718.
[4] D. Texier, J. Milanese, M. Jullien, J. Genée, J.-C. Passieux, D. Bardel, E. Andrieu, M. Legros, J.-C. Stinville, Strain localization in the alloy 718 Ni-based superalloy: from room temperature to 650 °C, Acta Mater. 268 (2024) 119759, https://doi.org/10.1016/j.actamat.2024.119759.
[5] M. Jullien, R.L. Black, J.C. Stinville, M. Legros, D. Texier, Grain size effect on strain localization, slip-grain boundary interaction and damage in the alloy 718 Ni-based superalloy at 650 °C, Mater. Sci. Eng., A 912 (2024) 146927, https://doi.org/10.1016/j.msea.2024.146927.
[6] T.G. Langdon, The physics of superplastic deformation, Mater. Sci. Eng., A 137 (1991) 1–11, https://doi.org/10.1016/0921-5093(91)90312-B.
[7] T.G. Nieh, J. Wadsworth, F. Wakai, Recent advances in superplastic ceramics and ceramic composites, Int. Mater. Rev. 36 (1991) 146–161, https://doi.org/10.1179/imr.1991.36.1.146.
[8] T. Watanabe, Grain boundary sliding and stress concentration during creep, Metall. Trans. A 14 (1983) 531–545, https://doi.org/10.1007/BF02643771.
[9] S. Wei, C.C. Tasan, On the plastic deformation of a CoCrFeNiW-C alloy at elevated temperatures: part II. Grain boundary sliding and damage mechanisms, Acta Mater. 252 (2023) 118898, https://doi.org/10.1016/j.actamat.2023.118898.
[10] W.R. Cannon, The contribution of grain boundary sliding to axial strain during diffusion creep, Philos. Mag. 25 (1972) 1489–1497, https://doi.org/10.1080/14786437208223868.
[11] I.M. Lifshitz, On the theory of diffusion-viscous flow of polycrystalline bodies, Sov. Phys. Jetp-USSR. 17 (1963) 909.
[12] W.A. Rachinger, Relative grain translations in the plastic flow of Al, J. Inst. Met. 81 (1952-1953) 33.
[13] S.-A. Shei, T.G. Langdon, A microstructural examination of the flow behaviour of a superplastic copper alloy, J. Mater. Sci. 16 (1981) 2988–2996, https://doi.org/10.1007/BF00540303.
[14] T.G. Langdon, An evaluation of the strain contributed by grain boundary sliding in superplasticity, Mater. Sci. Eng., A 174 (1994) 225–230, https://doi.org/10.1016/0921-5093(94)91092-8.
[15] M. Kini, A.H. Chokshi, The influence of titania on creep in superplastic zirconia, J. Am. Ceram. Soc. 93 (2010) 1725–1731, https://doi.org/10.1111/j.1551-2916.2010.03617.x.
[16] F.C. Liu, Z.Y. Ma, Contribution of grain boundary sliding in low-temperature superplasticity of ultrafine-grained aluminum alloys, Scr. Mater. 62 (2010) 125–128, https://doi.org/10.1016/j.scriptamat.2009.10.010.
[17] R.C. Gifkins, Grain-boundary sliding and its accommodation during creep and superplasticity, Metall. Trans. A 7 (1976) 1225–1232, https://doi.org/10.1007/BF02656607.
[18] A.E. Geçkinli, Grain boundary sliding model for superplastic deformation, Met. Sci. 17 (1983) 12–18, https://doi.org/10.1179/030634583790427504.
[19] R. Raj, M.F. Ashby, On grain boundary sliding and diffusional creep, Metall. Trans. A 2 (1971) 1113–1127, https://doi.org/10.1007/BF02664244.
[20] R.C. Gifkins, K.U. Snowden, Mechanism for viscous grain boundary sliding, Nature 212 (1966) 916–917, https://doi.org/10.1038/212916a0.
[21] M.F. Ashby, Boundary defects, and atomistic aspects of boundary sliding and diffusional creep, Surf. Sci. 31 (1972) 498–542, https://doi.org/10.1016/0039-6028(72)90273-7.
[22] M.F. Ashby, R. Raj, R.C. Gifkins, Diffusion-controlled sliding at a serrated grain boundary, Scripta Metall. 4 (1970) 737–741, https://doi.org/10.1016/0036-9748(70)90216-4.
[23] T.G. Langdon, Grain boundary sliding as a deformation mechanism during creep, Philos. Mag. 22 (1970) 689–700, https://doi.org/10.1080/14786437008220939.
[24] D. McLean, Grain boundary dislocations: their effect on vacancies and sliding, Philos. Mag. 23 (1971) 467–472, https://doi.org/10.1080/14786437108216396.
[25] R.C. Pond, D.A. Smith, On the absorption of dislocations by grain boundaries, Philos. Mag. 36 (1977) 353–366, https://doi.org/10.1080/14786437708244939.
[26] T. Watanabe, M. Yamada, S. Karashima, S. Shima, Misorientation dependence of grain boundary sliding in ⟨1010⟩ tilt zinc bicrystals, Philos. Mag. A 40 (1979) 667–683, https://doi.org/10.1080/01418617908234867.
[27] H. Kokawa, T. Watanabe, S. Karashima, Sliding behaviour and dislocation structures in aluminium grain boundaries, Philos. Mag. A 44 (1981) 1239–1254, https://doi.org/10.1080/01418618108235806.
[28] R.Z. Valiev, O.A. Kaibyshev, V.V. Astanin, A.K. Emaletdinov, The nature of grain boundary sliding and the superplastic flow, Phys. Status Solidi 78 (1983) 439–448, https://doi.org/10.1002/pssa.2210780209.
[29] H. Fukutomi, H. Takatori, R. Horiuchi, Grain boundary sliding with and without matrix slip deformation in Cadmium bicrystals, Trans. J. Inst. Met. 23 (1982) 579–584.
[30] A.I. Pshenichnyuk, V.V. Astanin, O.A. Kaibyshev, The model of grain-boundary sliding stimulated by intragranular slip, Philos. Mag. A 77 (1998) 1093–1106, https://doi.org/10.1080/01418619808221231.
[31] M.A. Linne, T.R. Bieler, S. Daly, The effect of microstructure on the relationship between grain boundary sliding and slip transmission in high purity aluminum, Int. J. Plast. 135 (2020) 102818, https://doi.org/10.1016/j.ijplas.2020.102818.
[32] N.V. Malyar, J.-S. Micha, G. Dehm, C. Kirchlechner, Dislocation-twin boundary interaction in small scale Cu bi-crystals loaded in different crystallographic directions, Acta Mater. 129 (2017) 91–97, https://doi.org/10.1016/j.actamat.2017.02.067.
[33] N.V. Malyar, B. Grabowski, G. Dehm, C. Kirchlechner, Dislocation slip transmission through a coherent Σ3{111} copper twin boundary: Strain rate sensitivity, activation volume and strength distribution function, Acta Mater. 161 (2018) 412–419, https://doi.org/10.1016/j.actamat.2018.09.045.
[34] B. Bellón, S. Haouala, J. Llorca, An analysis of the influence of the precipitate type on the mechanical behavior of Al - Cu alloys by means of micropillar compression tests, Acta Mater. 194 (2020) 207–223, https://doi.org/10.1016/j.actamat.2020.05.040.
[35] S. Lee, J. Do, B.G. Choi, U. Bansal, C. Kirchlechner, P.-P. Choi, S. Lee, Local plastic deformation in the vicinity of topologically close-packed phases in a Ni-based single crystal superalloy, Mater. Des. 250 (2025) 113600, https://doi.org/10.1016/j.matdes.2025.113600.
[36] M.D. Uchic, D.M. Dimiduk, J.N. Florando, W.D. Nix, Sample dimensions influence strength and crystal plasticity, Science 305 (2004) 986–989, https://doi.org/10.1126/science.1098993.
[37] N.V. Malyar, H. Springer, J. Wichert, G. Dehm, C. Kirchlechner, Synthesis and mechanical testing of grain boundaries at the micro and sub-micro scale, Mater. Test. 61 (2019) 5–18, https://doi.org/10.3139/120.111286.
[38] J.S. Weaver, N. Li, N.A. Mara, D.R. Jones, H. Cho, C.A. Bronkhorst, S.J. Fensin, G. T. Gray, Slip transmission of high angle grain boundaries in body-centered cubic metals: micropillar compression of pure Ta single and bi-crystals, Acta Mater. 156 (2018) 356–368, https://doi.org/10.1016/j.actamat.2018.06.046.
[39] J. Gong, A.J. Wilkinson, Sample size effects on grain boundary sliding, Scr. Mater. 114 (2016) 17–20, https://doi.org/10.1016/j.scriptamat.2015.11.029.
[40] Z.H. Aitken, D. Jang, C.R. Weinberger, J.R. Greer, Grain boundary sliding in aluminum nano-bi-crystals deformed at room temperature, Small 10 (2014) 100–108, https://doi.org/10.1002/smll.201301060.
[41] J. Luster, M.A. Morris, Compatibility of deformation in two-phase Ti-Al alloys: dependence on microstructure and orientation relationships, Metall. Mater. Trans. A 26 (1995) 1745–1756, https://doi.org/10.1007/BF02670762.
[42] D.M. Dimiduk, M.D. Uchic, T.A. Parthasarathy, Size-affected single-slip behavior of pure nickel microcrystals, Acta Mater. 53 (2005) 4065–4077, https://doi.org/10.1016/j.actamat.2005.05.023.
[43] N.V. Malyar, J.S. Micha, G. Dehm, C. Kirchlechner, Size effect in bi-crystalline micropillars with a penetrable high angle grain boundary, Acta Mater. 129 (2017) 312–320, https://doi.org/10.1016/j.actamat.2017.03.003.
[44] C. Herring, Diffusional viscosity of a polycrystalline solid, J. Appl. Phys. 21 (1950) 437–445, https://doi.org/10.1063/1.1699681.
[45] R.L. Coble, A model for boundary diffusion controlled creep in polycrystalline materials, J. Appl. Phys. 34 (1963) 1679–1682, https://doi.org/10.1063/1.1702656.
[46] H.-S. Nam, D.J. Srolovitz, Effect of material properties on liquid metal embrittlement in the Al–Ga system, Acta Mater. 57 (2009) 1546–1553, https://doi.org/10.1016/j.actamat.2008.11.041.
[47] S.X. McFadden, R.S. Mishra, R.Z. Valiev, A.P. Zhilyaev, A.K. Mukherjee, Low-temperature superplasticity in nanostructured nickel and metal alloys, Nature 398 (1999) 684–686, https://doi.org/10.1038/19486.
[48] R.K. Islamgaliev, R.Z. Valiev, R.S. Mishra, A.K. Mukherjee, Enhanced superplastic properties in bulk metastable nanostructured alloys, Mater. Sci. Eng., A 304–306 (2001) 206–210, https://doi.org/10.1016/S0921-5093(00)01440-4.

[49] I.A. Ovid'ko, A.G. Sheinerman, Grain boundary sliding, triple junction disclinations and strain hardening in ultrafine-grained and nanocrystalline metals, Int. J. Plast. 96 (2017) 227–241, https://doi.org/10.1016/j.ijplas.2017.05.005.
[50] S.X. McFadden, A.P. Zhilyaev, R.S. Mishra, A.K. Mukherjee, Observations of low-temperature superplasticity in electrodeposited ultrafine grained nickel, Mater. Lett. 45 (2000) 345–349, https://doi.org/10.1016/S0167-577X(00)00131-2.
[51] Y. Ishida, Boundary dislocations in coincidence site lattice grain boundary, Trans. Jpn. Inst. Met. 11 (1970) 107–112, https://doi.org/10.2320/matertrans1960.11.107.